diffusion-fundamentals.org

The Open-Access Journal for the Basic Principles of Diffusion Theory, Experiment and Application

DNA under confinement and the use of DNA as confinement

Hergen Brutzer[1], Evgeni Sperling[2], Katrin Günther[2], Jasmina Dikic[3], Friedrich Schwarz[1], Daniel Klaue[1], Frank Cichos[4], Michael Mertig[2,5#], Ralf Seidel[1,3,4§]*

[1]Biotechnology Center, Technische Universität Dresden, Dresden, Germany
[2]Physikalische Chemie, Mess- und Sensortechnik, Technische Universität Dresden, Germany
[3]Institute for Molecular Cell Biology, Westfälische Wilhelms-Universität Münster, Münster, Germany
[4]Institute for Experimental Physics I, Universität Leipzig, Leipzig, Germany
[5]Kurt-Schwabe-Institut für Mess- und Sensortechnik e.V. Meinsberg, Waldheim, Germany
*frank.cichos@physik.uni-leipzig.de, #michael.mertig@tu-dresden.de,
§ralf.seidel@physik.uni-leipzig.de

Abstract

In living systems DNA is subjected to considerable confinement but the molecule acts itself also as a confinement mechanism for cellular structures. Here we present investigations that study DNA under the confinement of supercoiling and within nanofluidic channels. Furthermore, we use DNA to confine the motion of microscopic and nanoscopic objects. In particular, we show how the motion dynamics of DNA-attached magnetic particles under external tension is affected and how DNA can confine the diffusion of enzymes to one dimension to follow the DNA contour.

Keywords: DNA, confinement, supercoiling, DNA electrostatics, DNA bendability, nanochannels, soft lithography, power-spectral-density analysis, protein diffusion

1 Introduction

In most organisms the conformation of DNA is significantly confined, i.e. the compartment that comprises the genomic information is considerably smaller than the radius of gyration of the stored DNA molecule in absence of any outer or internal constraints. For example, the genome of the bacterial model organism *Escherichia coli* (*E. coli*) comprises $6 \cdot 10^6$ bp. For the corresponding length of ~ 2 mm a radius of gyration R_G of ~ 7 µm is obtained (from $R_\mathrm{G} = (p \cdot L/3)^{1/2}$, with $p = 50$ nm being the persistence length and L the contour length of DNA), while the diameter of an *E. coli* cell measures about 1 µm. Correspondingly, the 2 m of DNA in human cells with a R_G of ~ 200 µm have to fit into the cell nucleus of ~ 10 µm in diameter. Biological systems use different mechanisms to reduce the entropic pressure when trying to hold the genomic DNA in its compartment. This includes DNA condensation by multi-valent ions, DNA supercoiling (DNA twisting) and DNA packaging by accessory proteins, which all can be considered as an internal confinement. Additionally, DNA itself confines the motion of attached

binding partners, such as DNA binding proteins, that often use DNA as a track to move on a pseudo-one-dimensional path through the cellular interior.

Here we investigate several aspects of DNA confinement and of the confining properties of DNA. In particular, we investigate DNA confinement by supercoiling, where extended superhelical plectoneme structures form when twisting DNA, and DNA confinement within nanofluidic channels. Furthermore, we study how the motion of a magnetic particle is affected by tethering through an attached DNA molecule. The results of these experiments provide a new method for the calibration of forces in magnetic tweezers. Finally, we develop a hybrid instrument that combines magnetic tweezers and total-internal-reflection-fluorescence (TIRF) microscopy to directly image stretched DNA molecules under tension and twist. We apply this device to investigate the diffusion of the restriction enzyme BcnI along DNA and study the influence of divalent ions on this process.

The presented experiments were obtained in the framework of the DFG-funded research unit FOR 877 “From Local Constraints to Macroscopic Transport”. This report summarizes the most important findings. Experimental details and more extensive explanations/discussions are provided in the original articles that are cited correspondingly in the text below.

2 DNA confinement by supercoiling

DNA twisting, the so-called supercoiling, is used in bacteria to compact the genomic DNA. To study the behavior of DNA upon supercoiling in a pure experimental system, we applied magnetic tweezers (Figure 1a). A DNA molecule is attached at one end to the bottom glass slide within a fluidic cell and at the other end to a superparamagnetic bead. A pair of magnets above the fluidic cell is used to exert a force in vertical direction onto the bead and thus the DNA. Since the magnetic beads are slightly anisotropic when magnetized, rotating the magnets allows to turn the beads and thus to supercoil the DNA [1, 2]. When twisting DNA under tension, the DNA length remains initially constant, while the torque within the molecule is linearly increasing (Figure 1c). When a critical torque is reached, the molecule buckles leading to an abrupt reduction of both the DNA length [1, 3] and the torque (Figure 1c). During buckling an initial plectonemic superhelix is formed (Figure 1a). When further twisting the DNA, the plectoneme is growing, providing a linear decrease of the molecule length with the applied turns while the torque remains constant. The abrupt DNA length and torque changes during buckling are due to an energetic penalty accompanying the extrusion of the initial plectoneme [1]. We previously showed [1] that buckling transition depends on the applied force, but more importantly on the ionic strength of the solution (Figures 1c, d). The latter is due to the fact that the energy to elongate the plectoneme is highly salt dependent, since the tightly wrapped DNA helices within the plectoneme exhibit significant electrostatic repulsions in particular at low ionic strength. At low salt (30 mM Na^+) the plectoneme-elongation energy is in the order of the energy required for the initial plectoneme extrusion, such that the buckling almost disappears (Figure 1d). At high salt the plectoneme elongation energy is considerably lower than the plectoneme extrusion energy due to the reduced electrostatic repulsion. This causes a well pronounced energetic penalty and thus a well pronounced buckling step. We developed a theoretical model that considers the different energetic contributions within the plectoneme and allows to predict the slope of the supercoiling curve and the torque in the postbuckling phase [4].

This model was confirmed by Monte-Carlo (MC) simulations (collaboration with the group of Gero Wedemann, Stralsund).

Here we further refined the input parameters of the MC simulations to study the bendability of DNA at large angles [5]. This was motivated by an ongoing debate in the recent years whether the energy required to introduce large curvatures into DNA can still be described by a harmonic model (the so-called worm-like-chain (WLC) model). A number of studies in the past indicated that for large curvatures significantly less energy would be required than assumed in the harmonic case [6]. For the latter, the bending energy E_{WLC} can be written as:

$$E_{\mathrm{WLC}} = \frac{1}{2} pL \cdot k_{\mathrm{B}} T \cdot \kappa^2, \tag{1}$$

where L is the DNA segment length, k_{B} the Boltzmann constant, T the temperature and κ the curvature (inverse of local bending radius). Using in the MC simulations, appropriate values for the effective DNA charge [4] and the DNA twist persistence length [5] allowed to reproduce the experimentally determined DNA supercoiling curves across the whole range of forces and salt concentrations applied (Figure 1). The position and the extent of the buckling as well as the slope in the postbuckling phase were in quantitative agreement when using the bending energy term of the WLC model [5]. We next tested an alternative model, the linear so-called sub-elastic-chain (LSEC) model, in which the bending energy would be given by:

$$E_{\mathrm{LSEC}} = \alpha \cdot k_{\mathrm{B}} T \cdot L|\kappa|. \tag{2}$$

While this model reproduced the slopes of the supercoiling curves in the postbuckling phase, it failed to describe the buckling transition. Buckling occurred earlier and much less pronounced than experimentally observed [5]. For moderate curvatures as occurring in plectonemes both models describe the DNA bending energetics reasonably well, while at high curvatures as occurring in the initial loop of the plectoneme only the WLC model appears to be the correct. The initial loop of the plectoneme can be much smaller than the DNA persistence length and can reach loop sizes that are frequently introduced by proteins into the DNA (Figures 1e, f). Thus, our supercoiling experiments allow to provide conditions at which deviations from the WLC model should become apparent and be of biological relevance. Under our experimental conditions, the WLC model holds even for extreme curvatures. In a recent report, significant deviations to the WLC bending energetics were found in single-molecule fluorescence experiments [7]. This may be explicable, considering that in our experiments significant positive torque is applied that keeps the DNA double-helix in its wound, intact state. In absence of torque spontaneous DNA fluctuations that lead to local unwinding or denaturation of base pairing may cause an apparent decreased bendability. Thus, while for intact double-strand DNA the WLC bending energetics is fully applicable, such fluctuations may cause an average softening at high curvature.

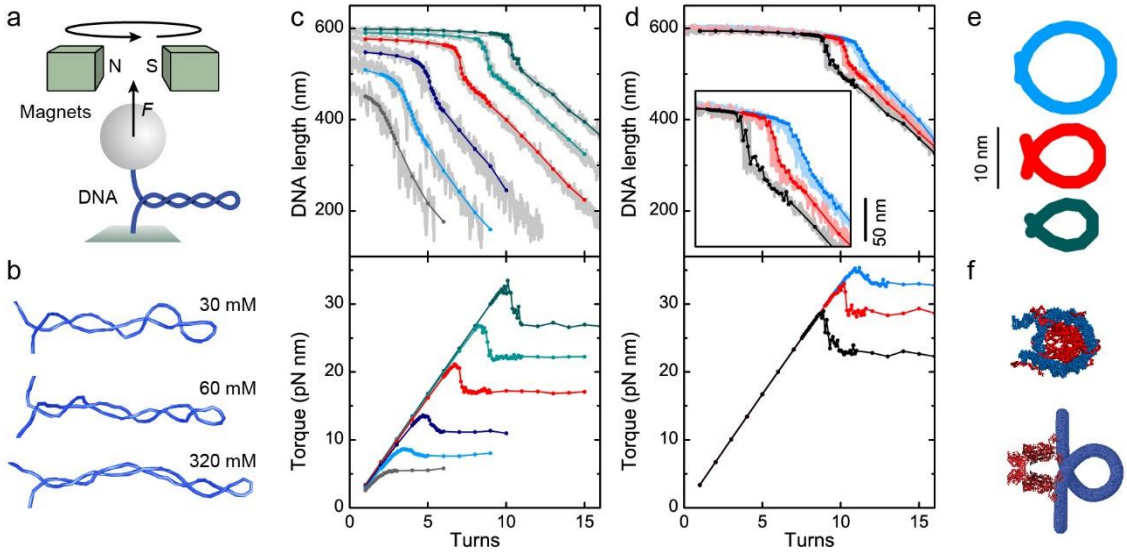

Figure 1: DNA supercoiling at different external tension and ionic strength. a) Experimental configuration. b) Snapshots of plectonemes from MC simulations at 1 pN force and different monovalent salt concentrations. DNA length and torque versus turns are shown in c) as function of the applied force (0.25, 0.5, 1.0, 2.0, 3.0, and 4.0 pN from bottom to top) and in d) for different monovalent salt concentrations (30, 60, and 320 mM in gray, red and blue, respectively). e) Initial-loop conformations from average bending angles at 0.5, 2, and 4 pN. Lines with filled circles represent data from MC simulations, while light gray curves show experimental data. f) Visualization of a nucleosome based on PDB entry: 1KX5 (top) and a model of the Lac repressor (bottom) derived from PDB entry: 1JWL. Biological models are to scale with end-loops shown in e. Figures are taken from Ref. [5].

The results from the single-molecule experiments in combination with theoretical modelling and MC simulations suggest that DNA supercoiling under tension can be fully understood by assuming WLC bending energetics and by approximating DNA as a cylinder to describe the electrostatic interactions of the molecule within the plectoneme in presence of monovalent ions. To challenge our model further, we investigated DNA supercoiling in presence of different cations in particular K^+, Na^+ and Li^+. This was motivated by the observation that DNA translocation through solid-state nanopores in presence of an external electric field is highly dependent on the cation radius [8]. While in presence of K^+ the DNA translocation is fastest, it is slightly slowed down for Na^+ and severely slower in presence of Li^+. To investigate whether this is due to a static effect, in which the screening layer around the DNA is altered, or a dynamic effect, in which the residence time of the counter ions at the DNA backbone is dependent on the ion species [8], we carried out supercoiling experiments in presence of 1 M of these cations (Figure 2a, see Ref. [9] for data at different forces). The obtained supercoiling curves provided very similar values for the DNA length before buckling and the slope after buckling (see also Ref. [9]). The position of the buckling transition (in number of applied turns) was similar for K^+ and Na^+. In presence of Li^+ the buckling position was however shifted by about two turns to higher turn numbers (Figures 2a, b). Also the length of the abrupt shortening was markedly increased (Figure 2c). The altered buckling in presence of Li^+ was consistently observed in multiple repetitions of the experiment, where typically measurements for the different cations were carried out on one and the same DNA molecule.

To elucidate the origin of this observation, force-extension measurements between 0.1 and 10 pN were carried out (see Ref. [9]). For double-strand DNA, the force-extension behavior in this force range is dominated by entropic bending fluctuations. By fitting the data with a WLC-based theoretical model [10], the persistence length of the DNA can be precisely determined. For the high ionic strengths that were applied in the supercoiling experiments we obtained for both Na^+ and Li^+ DNA persistence lengths

of 41 nm (K^+ not studied). As expected, this value is reduced compared to the 50 nm obtained at physiological salt concentrations, due to the reduced electrostatic repulsion of neighbouring DNA segments. However, the DNA bending rigidity is not affected by the type of the cation. The slope of the supercoiling curve after buckling is a result of minimized DNA bending in competition to minimized electrostatic DNA-DNA interactions in the plectoneme. Considering that the slope and the bending rigidity are not affected by the type of the cation, this strongly suggests that the electrostatic DNA-DNA interactions within the plectoneme are also not cation dependent. Therefore, the observed cation dependence of the buckling transition is most likely due to an altered energetics when forming the initial loop of the plectoneme. From analysing the width of the buckling transition [1, 9], we also determined the number of turns that got absorbed by the initial plectoneme loop during buckling. It was about 1.7 turns and within error independent of the cation type. Given that the DNA length decrease during buckling was increased for Li^+, this suggests that the initial plectoneme loop is larger, i.e. in presence of Li^+ it is energetically more costly to force a high DNA curvature. This is interesting, since the low curvature entropic bending fluctuations, as characterized in the force-extension measurements, are not affected by the cation type. The microscopic origin of this behavior is currently unclear. Potentially the ion size plays also here a significant role. We hypothesize that larger ions cannot be well accommodated within the grooves of the bent DNA.

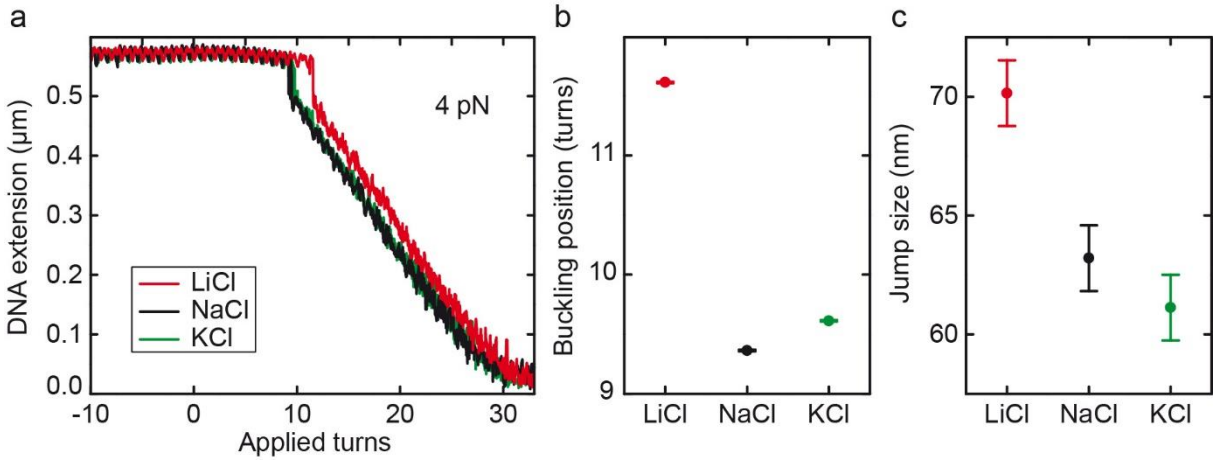

Figure 2: Dependence of DNA supercoiling on the type of counterion. a) DNA supercoiling curves in presence of 990 mM LiCl (red), NaCl (black), or KCl (green) in 10 mM TRIS-HCl at pH 8.0. b) Position of the abrupt buckling transition for the different cations at 4 pN. c) Length of the abrupt DNA shortening for the different cations at 4 pN. See Ref. [9] for additional data (e.g. additional forces) and further details.

3 DNA confinement in nanofluidic channels

Effects of spatial confinement on DNA conformation are not only of interest in a biological context but also for applications in DNA nanotechnology, e.g. genome mapping [11] and DNA separations. We adapted the soft-lithographic technique [12] for the fabrication of re-usable, inexpensive and non-collapsing sub-micrometer wide channels with stepwise changing cross-sections down to the 100-nm range. Double-stranded DNA (dsDNA) molecules are electrophoretically forced to enter the channels under partial uncoiling [13].

For the fabrication of nanofluidic systems, a variety of both materials and techniques have been applied. The traditional inorganic materials like fused silica, glass and silicon allow the application of

well-established patterning methods such as laser-interference lithography or electron-beam lithography and of related etching processes. Consequently, patterning of those substrates is time consuming and requires expensive clean room facilities. Moreover, silicon is non-transparent for visible light, and therefore, not suitable in optical experiments. In contrast, molding a silicon master with organic polymers, e.g. polydimethylsiloxane (PDMS) or Poly(methyl methacrylate) (PMMA) results in optical transparent and biocompatible fluidic devices that can be produced in a stanpostsdard laboratory. Here we report on the soft-lithographic fabrication of nanochannels, using a bi-layered polymer replica that is characterized by robustness, transparency, low cost and reusability.

So far, soft lithographically fabricated micro- and nano-structures for the study of DNA in confining geometries [14, 15] are composed of PDMS (Sylgard 184, Dow Corning) or so-called *hard*-PDMS [16] and bonded to a cover glass as carrier. The application of those cross-linked polymers for molding nanostructures, however, is limited due to their mechanical properties, in particular due to their low Young's modulus (Sylgard 184: ~ 2 MPa, *hard*-PDMS: ~ 9 MPa [16]) compared to glass (~ 70 000 MPa [17]). As a consequence, for both kinds of PDMS, roof-collapse due to adhesion between the elastomer nanostructure and the glass substrate may occur in the entrance regions of the microfluidic system (Figure 3), where the width-to-height ratio becomes large. Therefore, in addition to *hard*-PDMS, here the anorganic-organic hybrid polymer *Ormostamp* (micro resist technology GmbH), possessing a Young's modulus of ~ 650 MPa [18, 19], in combination with PDMS is successfully applied for the UV-based imprint fabrication of non-collapsing, transparent nanochannels.

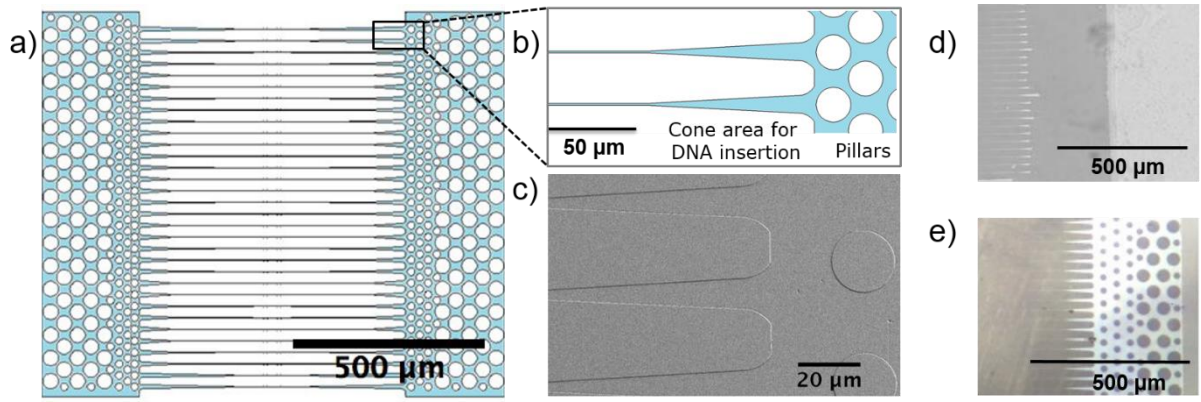

Figure 3: a) Scheme of the master structure with pillars in the entrance regions, tapered intermediate areas leading to the nanochannel area in the center of the fluidic device. The widths of the nanochannels are stepwise narrowed with the smallest cross-section located in the center, being quadratic in this case. b) Zoom-in into the inner pillar region and the intermediate tapered area. c) SEM image of the *Ormostamp* replica displaying the perfect molding. Light microscopic image of a 175-nm structure with mounted cover glass depicting posts and entrance region for d) a *hard*-PDMS replica, resulting in a collapsed structure and e) an *Ormostamp* replica that remains intact.

The silicon masters of all structures (Figure 3a) consist of a nanochannel array of varying lengths in the center of the structure comprising 32 individual nanochannels associated with tapered intermediate channel regions on both sides of the nanochannels. Those are bounded by pillar areas, intended for dispersion of entangled DNA molecules. The nanochannel array itself is stepwise narrowed in width, each section has a length of 100 µm. That allows to vary the DNA confinement for one and the same molecule. The 100-nm channel structure narrows from 1000 nm at the channel entrance over 500 nm

and 300 nm to 100 nm width in the center of the structure. In this case the height of the channels is 100 nm, meaning that the channels have a quadratic cross-section in the center.

In the following, the fabrication of nanochannels with smallest dimensions of 375 nm, 175 nm and 100 nm using the newly developed replication approach is described. The polymer replicas are built by two interconnected polymer layers: a block-like one, made of the soft PDMS Sylgard 184 with a thickness of a few millimetres, absorbing mechanical stress and acting as carrier and a micrometre-sized layer of either *Ormostamp* or *hard*-PDMS containing the nanochannels. Due to different adhesive and cross-linking properties of *Ormostamp* and *hard*-PDMS, the fabrication procedures are different. Figure 4 depicts schematically the fabrication process of the channels with a size of 100 nm and 175 nm.

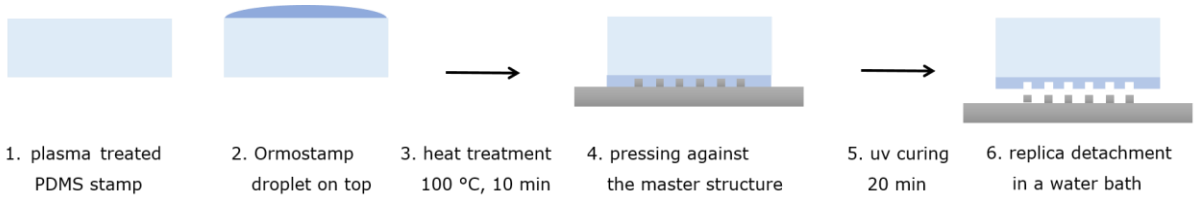

Figure 4: Scheme of the *Ormostamp* replica fabrication process.

The surface of the PDMS “pillow” is activated by an air plasma treatment for about 1 min (Plasma Prep III, SPI Supplies) to achieve a hydrophilic surface, then a small droplet of *Ormostamp* is deposited on top and subsequently treated at 100 °C for about 10 min. The heat treatment allows for chemical binding of *Ormostamp* to the PDMS support. Thereafter, the composite is pressed manually with tweezers onto the silicon master and is cross-linked by UV radiation (UV-lamp Dermalight 80, Dr. Hönle, main emission peak at 311 nm) for about 20 min; no mechanical stress is applied during UV radiation. Detachment of replica and master is achieved using a water bath that decreases the surface adhesion between the two.

Hard-PDMS is used for replication of the 375-nm structure. Here first a small droplet of the *hard*-PDMS mixture is placed on the silicon master structure covering the channel area completely, then the Sylgard 184 mixture (common ratio of polymer base to cross linker of 10:1) is deposited on top; no bulk intermixing occurs during the short processing time due to the high viscosity of PDMS [13]. Cross-linking is achieved by thermal curing 90 °C for about 20 min.

The surface properties of both the *hard*-PDMS and the *Ormostamp* replica were characterized by atomic force microscopy (Cypher, Asylum Research). The rms-roughness is with 0.2 nm to 0.5 nm comparable to a silicon wafer having a rms value of ∼ 0.2 nm [20]. The nanochannel geometry of the silicon master with the stepwise narrowing is well reproduced (Figure 5).

Finally, the nano-structures were sealed with cover slides (Menzel) possessing 30 nm-thick platinum electrodes on opposite edges. To this end, both cover slide and replica were pre-cleaned with absolute ethanol, dried and air plasma treated. Mounting glass and nanostructured replica is followed by a last thermal curing step improving the adhesion (for details see [13]). The assembly is then ready for studies on the influence of strong confinement on the transport properties and the conformational behavior of dsDNA.

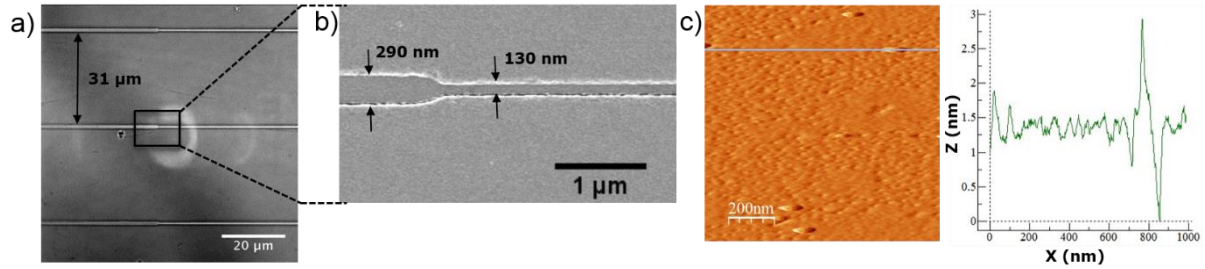

Figure 5: Nanostructure *Ormostamp* replica: a) Optical micrograph. b) Scanning electron micrograph. c) Scanning force micrograph of the smooth surface (left) with height profile (right).

In sub-micrometer fluidic channels, DNA is strongly confined if the channel width is less than the size of the entropic coil which is characterized by the root-mean-squared end-to-end distance $< R^2 >^{1/2} = (2pL)^{1/2}$, where L denotes the DNA contour length and p the persistence length. For the here used λ-phage DNA (*New England Biolabs*) with a length of 16.3 µm, a coil of about 1.3 µm is formed, and therefore, the prepared nanochannels provide strong confinement.

0.9 nM λ-DNA in 0.5x TAE buffer, pH 8.0 was stained with the bis-intercalating dye YOYO-1 (*Life Technologies*) at a ratio of 1 dye per 7.5 base pairs. For this staining ratio, we expect an increased contour length of 19.6 µm due to dye intercalation [21]. To increase the solution viscosity, 2 wt% of the water soluble polymer polyvinylpyrrolidon (PVP, M = 40 kg/mol) was added. Moreover 1 vol% mercaptoethanol was added for the reduction of photo-bleaching.

Filling the nanochannels with the DNA containing buffer solution is achieved due to capillary action by placing a volume of app. 5 µl on the entrance region of both sides of the polymeric fluid system (Figure 6).

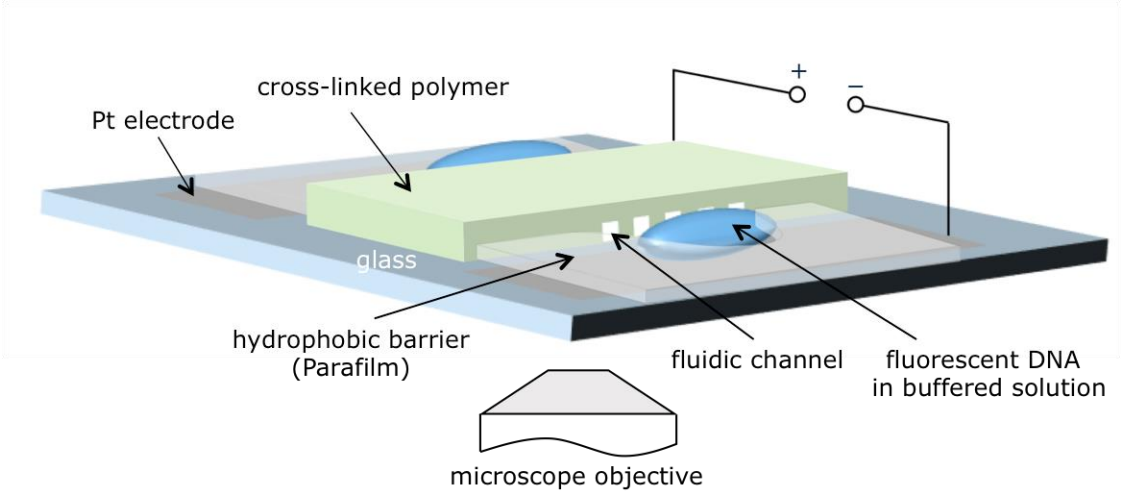

Figure 6: Experimental setup for electrophoretic manipulation of single DNA molecules.

Non-fragmented µm-long DNA molecules itself will not enter the channels, unless they experience a force that overcomes the entropic coiling. To this end, DNA is driven into the nanochannel region by applying an electrical field of app. 100 V/cm via the platinum electrodes (Figure 6). The electrical field is controlled by a source-measurement unit (*Keithley 2602B*, Keithley Instruments) and manual probe heads *PH100* (Suss Microtec). For image acquisition, an inverted microscope Axiovert 200 M (Zeiss)

equipped with a 100x oil immersion objective (NA 1.45) and a back-illuminated CCD camera (Cascade 512B, Photometrics) was employed. The images were processed using *ImageJ* [22].

In a typical experiment, DNA was forced to enter the nanochannel section by applying an electrical field, and subsequently, stopped by lowering the applied voltage, immediately after the DNA entered the nanochannel. We were then able to observe molecule stretching (Figure 7).

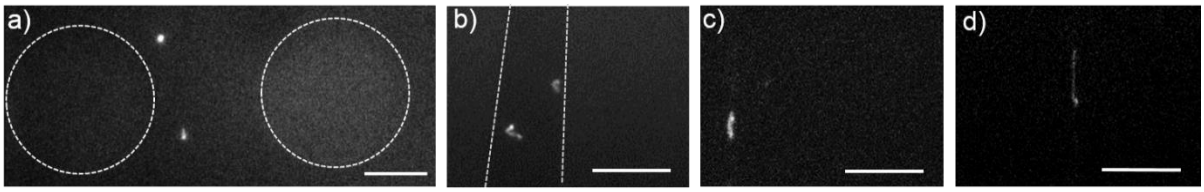

Figure 7: Fluorescence microscopy images of DNA molecules. DNA molecules entered different regions of the 175-nm structure by application of an electrical field of app. 100 V/cm and were captured by reducing the voltage to a few V/cm for compensation of hydrodynamic flow. The scale bar corresponds to 10 µm. a) Pillar region: DNA is still in a coiled conformation. b) Intermediate region: DNA is slightly uncoiled. c) Nanochannel area: DNA is stretched to app. 19 % of its contour length. d) If one end of the DNA molecule is non-permanently immobilized at channel surface impurities, stretching of app. 40 % was observed.

Currently, we observe molecule stretching to an average length of app. 19 % of its contour length. The achieved degree of stretching is compared with measurements by Guo *et al*., they reported in their imprinted nanofluidic channels for a cross-section of 300 nm × 700 nm a stretching of YOYO-stained T5 phage DNA of 15 % [23]. Therefore, we assume that the recorded molecules are not yet in the narrowest nanochannel region, but in the 175 nm × 1000 nm section of the 175-nm structure.

Furthermore, not only the degree of stretching, but also the dynamics of length and intensity fluctuations were monitored as it is exemplarily depicted in the kymograph for a DNA molecule captured in the 175 nm × 1000 nm section of a 175-nm channel nanostructure (Figure 8a).

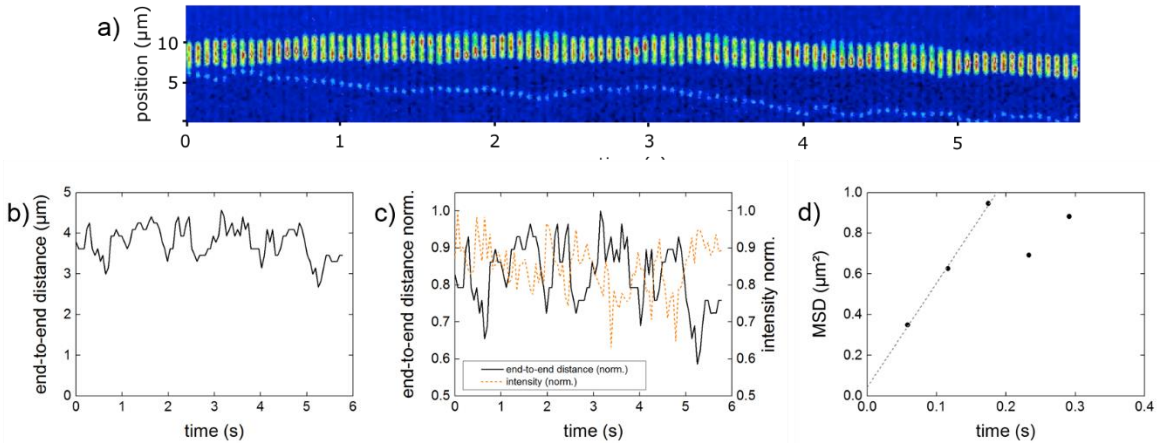

Figure 8: Analysis of an individual DNA molecule confined in the 175 nm × 1000 nm section of a 175 nm-channel nanostructure a) Kymograph for a time interval of 5.8 s. The molecule is stretched to an average end-to-end distance of 3.8 µm. Color codes the fluorescence intensity: regions of high intensity are red. b) End-to-end distances versus time demonstrating length fluctuations. c) Molecule lengths and intensities, both displayed normalized, show an inverse behavior. d) Mean squared displacement of supposedly diffusing intensity maxima; the dashed line shows a linear fit in the interval of 0 to 0.2 s indicating a preliminary determined diffusion coefficient in the order of 2.5 µm²/s.

Both length and intensity fluctuations reflect conformational variations of the captured molecule. The fluctuations in length can be quantified in terms of the standard deviation of the end-to-end distance for the particular degree of confinement. For the here depicted molecule, we determined a mean end-to-end distance of 3.8 µm and a standard deviation of 0.4 µm, i.e. about 10 % (Figure 8b). The appearance of intensity maxima and the visible length of the molecule are correlated (Figure 8c). The appearance of spots with high intensity correspond to a decrease of the length of the molecule. The intensity maxima, red-coloured in the kymograph (Figure 8a), depict regions with a higher local DNA density that apparently move along the DNA contour. We assume that those regions of higher density can either diffuse along the contour of the molecule or they develop and vanish during observation. Supposing the first case, an, estimation of the one-dimensional mean squared displacement (MSD) indicates a diffusion coefficient of 2.5 µm²/s. This is faster than the diffusion of plectonemes along the DNA reported by Loenhut et *al*. in a special magnetic tweezers setup. They found the diffusion influenced by salt concentration and applied forces: decreasing both increases the diffusion [24]. With a stretching force of app. 22 fN, we apply less force and no additional salt is added compared to [24]; so a larger diffusion coefficient is reasonable. We conclude that the chosen channel design providing different cross sections will enable to elucidate the underlying mechanism for the DNA density fluctuations.

4 Confined motion of a DNA-attached particle under external force

As an example for the confining properties of DNA, we investigated how the motion of a magnetic particle is attached by an attached DNA tether (Figure 9). This is highly relevant for magnetic tweezers experiments, since the fluctuations of the magnetic bead perpendicular to the force direction are used to calibrate the applied magnetic force. In typical magnetic tweezers experiments the force acts in the vertical direction along the optical axis of the microscope, while the actual magnetic field is oriented in the horizontal (further referred to as lateral) direction. Due to the attached DNA tether the magnetic particle moves due to Brownian fluctuations in a pendulum geometry. However, the applied magnetic microbeads exhibit a magnetization anisotropy, such that they align themselves with their preferred axis to the magnetic field. This results in two different pendulum geometries (see sketches in Figures 9a, b): For fluctuations along the magnetic field (further referred to as *y*-direction) the pendulum length equals the DNA length L due to the pinned bead orientation. In the horizontal direction perpendicular to the magnetic field lines (further referred to as x-direction) it equals the sum of L and the bead radius R, since the bead is free to rotate around its center axis in direction of the field.

When displacing the pendulum laterally along the short pendulum axis by a distance y, the back-driving force is given by $F_{\mathrm{y}} = -F_{\mathrm{mag}}/L \cdot y$. This expression is equivalent to the behavior of a Hookean spring with the spring constant $k_{\mathrm{y}} = F_{\mathrm{mag}}/L$. Using the equipartition theorem, one can write for the thermally induced mean square displacement of the pendulum along y:

$$E_{\mathrm{therm}} = \frac{1}{2} k_{\mathrm{y}} \langle y^2 \rangle = \frac{1}{2} k_{\mathrm{B}} T. \tag{3}$$

This directly provides the acting magnetic force using the lateral bead fluctuations:

$$F_{\mathrm{mag}} = \frac{k_{\mathrm{B}}T}{\langle y^2 \rangle} L. \tag{4}$$

In practice, the magnetic force is not directly obtained from the mean-square lateral displacement, but rather from the frequency spectrum of the displacement. The dynamics of a Hookean spring coupled to an element with viscous drag coefficient γ_{y} is described by a Lorentzian function for the power-spectral-density (PSD) [25]:

$$S_{\mathrm{y}}(f) = \frac{4k_{\mathrm{B}}T\gamma_{\mathrm{y}}}{k_y^2} \frac{1}{1 + (f/f_{\mathrm{c}})^2}, \tag{5}$$

where f is the frequency and the characteristic cut-off frequency $f_{\mathrm{c}} = k_{\mathrm{y}}/(2\pi\gamma_{\mathrm{y}})$. After calculating a PSD spectrum from a recorded time trajectory, the data is fitted with a modified form of Eq. 5 that comprises corrections for acquisition artifacts of the bead position (see Ref. [26] for full details). This provides k_{y} and γ_{y} and thus, respectively, also the applied force and the radius of the bead (using the Stokes relation). For the short pendulum geometry, forces can be precisely calibrated using this methodology. Recent high-resolution magnetic tweezers experiments demand however the use of short DNA molecules (tether length shorter than bead radius) [27], for which large cut-off frequencies can be obtained that may exceed the frequency of the bead position detection. At such conditions a reliable force calibration is impeded. To overcome this limitation the long pendulum geometry may be used for calibration, at which lower cut-off frequencies would be obtained. We therefore tested whether correct forces would be obtained for this geometry. To this end we recorded position trajectories of a magnetic bead with nominal radius of 0.52 µm that was attached to a 1.9 kbp long DNA molecule at an acquisition frequency of 2800 Hz by camera based particle tracking. PSD analysis for the short pendulum geometry provided a force of 4.84 $\pm$ 0.04 pN and a bead radius of 511 $\pm$ 2 nm (Figure 9a). When analyzing the PSD for the long pendulum geometry using as spring constant $k_{\mathrm{x}} = F_{\mathrm{mag}}/(L + R)$ and an adapted drag coefficient γ_{x} (see Ref. [26] for full details), significantly lower values for force and radius were obtained (4.59 $\pm$ 0.05 pN and 463 $\pm$ 2 nm, see Ref. [26] for data and full details).

Brownian dynamics simulations, which model the motion of the translational motion in all three dimensions and the rotation of a bead attached to a tether reproduced the experimental observations: correct forces and radii were obtained for the short pendulum geometry while too low values for these quantities were obtained for the long pendulum geometry (Figure 9a and Ref. [26]). The difference between the short and the long pendulum geometry are the additional rotational fluctuations of the magnetic bead for the latter case. Using a set of two coupled Langevin equations we derived a theoretical expression for the PSD of the coupled translational and rotational motion of the bead in the long pendulum geometry. This provided a more complex PSD that consisted of a sum of two Lorentzians:

$$S_{\mathrm{x}}^{\mathrm{coupl}}(f) = \frac{4k_{\mathrm{B}}T}{(2\pi)^2(1 + C^2\gamma_{\mathrm{x}}\gamma_{\varphi}/R^2)} \left(\frac{\gamma_{\varphi}C^2}{R^2} \frac{1}{f_+^2 + f^2} + \frac{1}{\gamma_{\mathrm{x}}} \frac{1}{f_-^2 + f^2} \right), \tag{6}$$

with $f_{\pm}$ being the two cut-off frequencies, γ_{φ} being the rotational drag coefficient of the bead and C being a function of F_{mag}, L, R, γ_{x} and γ_{φ} (see Ref. [26]). The new function of the PSD for the long pendulum geometry provides now correct forces and bead radii for the experimental and the simulated data (Figure 9b). We tested the new calibration method for the long pendulum geometry at different applied forces, bead radii and acquisition frequencies. For all conditions correct forces and radii were obtained. Depending on the DNA length considerably larger forces can be calibrated with this method as compared to the short pendulum geometry. Furthermore, we demonstrated that also the absolute force accuracy was improved [26]. Most likely this is due to the invariance of the method against underestimations of the DNA length. We note that the force calibration using the long pendulum geometry does not require additional fit parameters compared to the calibration based on the short pendulum geometry. We therefore recommend the use of this method on a routine basis. Overall, our results demonstrate that careful analysis of the dynamics of a DNA tethered particle allows to understand the underlying principles of its movement.

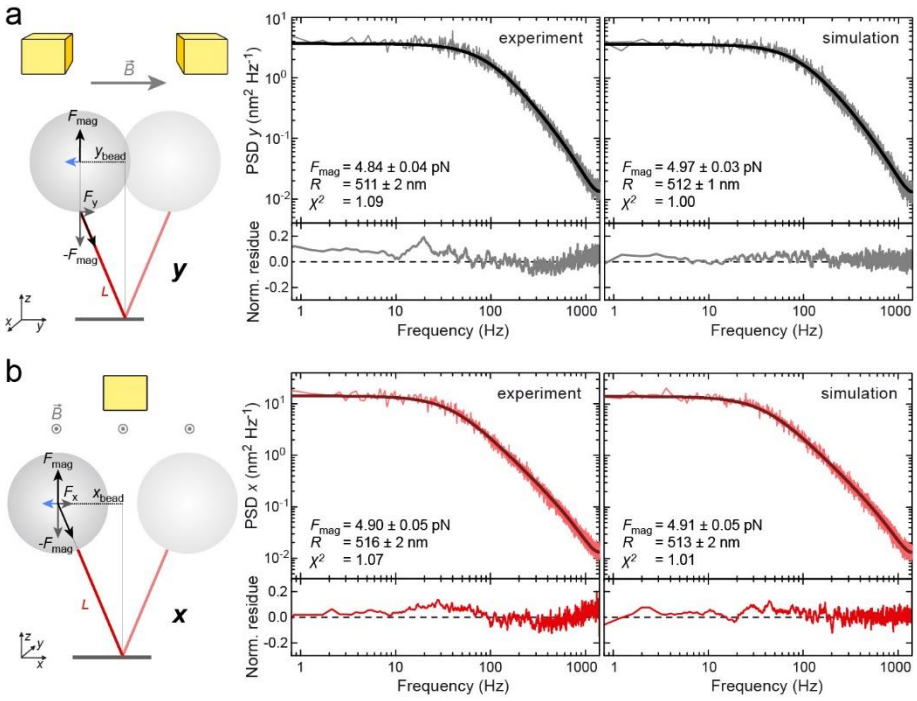

Figure 9: PSD analysis of the motion of a DNA attached magnetic particle. a) Short pendulum geometry. (*left*) Sketch of the lateral bead motion along the magnetic field lines, where the particle orientation is pinned. Results of the PSD analysis using the single-Lorentzian model (based on Eq. 5) are shown for experimental (*middle*) and simulated (*right*) data. The dark gray line represents the best fit to the data shown in light gray. Obtained fit parameters are given in the plot. b) Long pendulum geometry in which the particle is free to rotate. Sketch and plots are according to a. The data was fitted with the double-Lorentzian model based on Eq. 6. Figures were taken from Ref. [26].

5 One-dimensional diffusion along DNA

When studying the behavior of DNA under twist and tension (see Section 2) it is highly desirable to reveal the dynamics and the form of the plectonemic superhelices. This includes the number of plectonemic superhelices that are formed, their mobility along DNA and their dynamic formation and collapse. This dynamics cannot be obtained from the DNA length measurements. Similar to the lateral fluctuations of the magnetic bead, the dynamics of the vertical bead fluctuations along the DNA

stretching direction are dominated by the hydrodynamic drag of the bead itself. The minor contribution of the DNA hydrodynamics is essentially masked [28]. To reveal processes that are occurring on the DNA in real time we therefore developed a magnetic tweezers configuration that allows to stretch single DNA molecules in almost parallel orientation to the imaging plane and simultaneously to image fluorescently labeled objects on the DNA [29]. This experimental configuration uses a setup that combines magnetic tweezers and total-internal-reflection-fluorescence (TIRF) microscopy [30]. A miniature magnet stage conveniently allowed side-wards stretching of single DNA molecules that were immobilized within capillaries with quadratic cross-section (Figure 10).

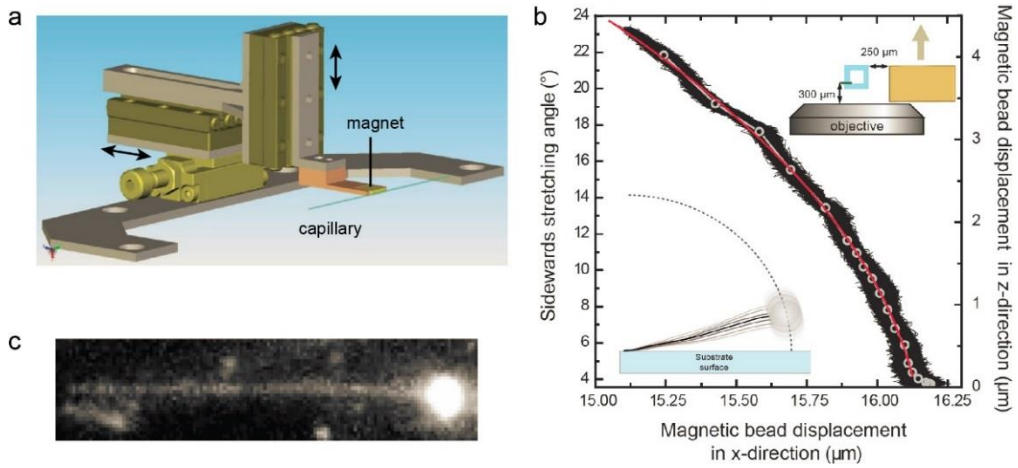

Figure 10: Sidewards stretching of a single DNA molecule and simultaneous fluorescence imaging. a) Magnet stage with two motorized stages that allow to move the magnet (indicated by arrows) laterally to a capillary with quadratic cross-section in which the experiments are performed. b) Variation of the stretching angle of a 16 µm long DNA molecule attached to a µm-sized bead by changing the magnet position. Black data points show all recorded bead positions, open circles the average bead position at a given magnet position. The sketch in the upper right corner illustrates the dimensions of the capillary and the magnet and the magnet movement. The sketch in the lower left corner illustrates the movement of the mean magnetic bead position when varying the magnet position. c) Fluorescence image of a stretched 16 µm long DNA molecule. The molecule was labelled with YOYO-1 and excited in TIRF geometry at 488 nm. For further details see Ref. [29] from which the images were taken.

Simultaneous fluorescence excitation using with a laser in objective-type TIRF geometry and imaging of the fluorescent signal using an EMCCD camera allowed to directly visualize the stretched DNA molecules when they were stained with a fluorescent dye (Figure 10c).

As a proof-of-principle that our technique allows to directly visualize processes that are ongoing on the DNA, we investigated the interaction of the monomeric restriction enzyme BcnI with DNA. Restriction enzymes are typically protein dimers that recognize few base-pairs long target sequences and subsequently cut the DNA at these sites. Each monomer is cutting one strand of the double helix to produce a full double-strand cut. BcnI belongs to a small class of monomeric restriction enzymes that use only one catalytic site to cut both DNA strands. From biochemical experiments it has been suggested that BcnI first binds the target sequence in one orientation to cut the first strand and uses diffusion along the DNA to leave the target site and then turns into the opposite orientation. After subsequent target binding the second strand will be cleaved [31]. A crucial observation that is needed to confirm the proposed mechanism for this enzyme is the ability of the enzyme to diffuse in one dimension along the DNA. Using BcnI molecules that were attached to single quantum dots, we could

observe the attachment and the motion of the enzyme along DNA (Figure 11a, [32]) applying our hybrid instrument combining magnetic tweezers and TIRF microscopy.

After attachment, enzymes were typically moving over long time periods along the DNA. The enzyme's mean-square displacement along DNA was linear in time confirming the diffusive nature of its motion (Figure 11b). Since divalent cations, in particular Mg^{2+}, are an essential cofactor for the DNA cleavage reaction, we studied the behavior of the enzyme in presence of Mg^{2+} and Ca^{2+} as well as in absence of divalent cations. While the diffusion coefficient was very similar for these different conditions, the interaction time of the enzyme was markedly shorter when Mg^{2+} or Ca^{2+} were present [32].

Overall, our hybrid instrument is well suitable to directly image processes on single stretched DNA molecules. Using the original magnet configuration (Figure 1a) additionally allows to apply supercoiling to stretched DNA. It can thus be readily applied to study details of the dynamics of plectonemes on DNA in addition to observations that became recently available [24].

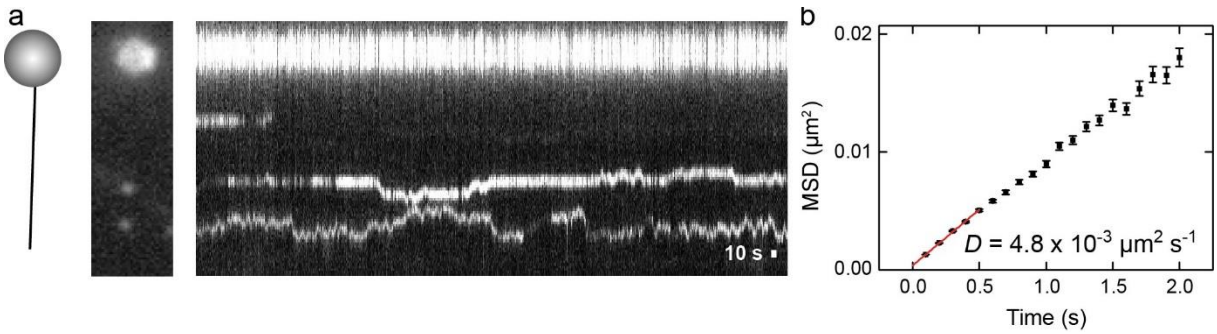

Figure 11: Diffusion of the monomeric restriction enzyme BcnI along DNA in absence of divalent ions. a) Kymograph (fluorescent intensity along the DNA over time) of the attachment/dissociation and movement of fluorescently labelled BcnI molecules on a single stretched DNA. On the left side a sketch of the configuration of DNA and bead and a single snapshot of the fluorescence image series are shown. In the latter, the autofluorescent magnetic bead and two attached BcnI molecules can be seen. b) Mean-square-displacement of individual enzyme complexes over time. A linear fit to the data (red line) provides a diffusion coefficient of $4.8 \cdot 10^{-3}$ µm^2 s^{-1}. See Ref. [32] for details.

6 Conclusion

In summary, we studied the influence of different confinements on the DNA conformation and also used DNA to confine the motion of attached objects.

The first type of confinement was external tension in combination with DNA supercoiling. Using MC simulations we could fully reproduce the experimentally observed change of the DNA length with applied turns for a multitude of conditions (tension, salt concentration). This allowed us to show that the mechanics of strongly bent DNA (end-loop of plectonemes) can still be explained by the conventional WLC model [5]. Furthermore, we observed that the mechanics of strong DNA bending is influenced by the type of the cation in solution [9].

The second type of confinement is provided by nanofluidic channels. The soft lithographically fabricated nanofluidic channel assemblies composed of a bi-layered polymer replica and a glass carrier display interesting features; they are robust, transparent and reusable. As a particular design attribute, the stepwise reduction of the nanochannel cross section will enable studies of one and the same molecule under changing the degree of confinement. DNA molecules are electrophoretically forced to enter confining areas of the fluid structures and monitored by fluorescence microscopy. First

observations reveal both a DNA stretching and fluctuations in both length and fluorescence intensity that are obviously related to intrinsic conformational alterations.

We furthermore investigated how the motion of magnetic beads is influenced by an attached DNA molecule. Using PSD analysis we could reveal the rotational motion of the particle around the magnetic field direction. The careful analysis of the particle motion provided the basis for an improved calibration of magnetic tweezers [26].

Finally, we used a hybrid instrument that combines magnetic tweezers and TIRF microscopy to image directly laterally stretched DNA. This allowed us to follow the diffusional motion of fluorescently labelled proteins along the DNA [32]. Likewise this assay can also be applied to study the behavior of dynamic DNA structures, such as the diffusion and the long-distance hopping of plectonemes.

Acknowledgements

The research reported in the manuscript has been supported by the Deutsche Forschungsgemeinschaft within project P2 “Static and dynamic properties of DNA-based polymer structures under constraints and confinement” of the Saxon Research Unit FOR 877 “From Local Constraints to Macroscopic Transport”.

References

[1] H. Brutzer, N. Luzzietti, D. Klaue, R. Seidel: *Energetics at the DNA supercoiling transition.* Biophys. J. **98**, 1267–1276 (2010)

[2] F. Mosconi, J.F. Allemand, D. Bensimon, V. Croquette: *Measurement of the torque on a single stretched and twisted DNA using magnetic tweezers.* Phys. Rev. Lett. **102**, 078301 (2009)

[3] S. Forth, C. Deufel, M.Y. Sheinin, B. Daniels, J.P. Sethna, M.D. Wang: *Abrupt buckling transition observed during the plectoneme formation of individual DNA molecules.* Phys. Rev. Lett. **100**, 148301 (2008)

[4] C. Maffeo, R. Schöpflin, H. Brutzer, R. Stehr, A. Aksimentiev, G. Wedemann, R. Seidel: *DNA-DNA interactions in tight supercoils are described by a small effective charge density.* Phys. Rev. Lett. **105**, 158101 (2010)

[5] R. Schöpflin, H. Brutzer, O. Müller, R. Seidel, G. Wedemann: *Probing the elasticity of DNA on short length scales by modeling supercoiling under tension.* Biophys J. **103**, 323–330 (2012)

[6] P.A. Wiggins, T. van der Heijden, F. Moreno-Herrero, A. Spakowitz, R. Phillips, J. Widom, C. Dekker, P.C. Nelson: *High flexibility of DNA on short length scales probed by atomic force microscopy.* Nat. Nanotechnol. **1**, 137–141 (2006)

[7] R. Vafabakhsh, T. Ha: *Extreme bendability of DNA less than 100 base pairs long revealed by single-molecule cyclization.* Science **337**, 1097–1101 (2012)

[8] S.W. Kowalczyk, D.B. Wells, A. Aksimentiev, C. Dekker: *Slowing down DNA translocation through a nanopore in lithium chloride.* Nano Lett. **12**, 1038–1044 (2012)

[9] H. Brutzer: *Mechanics and dynamics of twisted DNA*. Ph.D. thesis, TU Dresden (2013)

[10] C. Bouchiat, M.D. Wang, J. Allemand, T. Strick, S.M. Block, V. Croquette: *Estimating the persistence length of a worm-like chain molecule from force-extension measurements.* Biophys. J. **76**, 409–413 (1999)

[11] E.T. Lam, A. Hastie, C. Lin, D. Ehrlich, S.K. Das, M.D. Austin, P. Deshpande, H. Cao, N. Nagarajan, M. Xiao, P.-Y. Kwok: *Genome mapping on nanochannel arrays for structural variation analysis and sequence assembly*. Nat. Biotechnol. **30**, 10.1038/nbt.2303 (2012)

[12] G.M. Whitesides, E. Ostuni, S. Takayama, X. Jiang, D.E. Ingber: *Soft lithography in biology and biochemistry*. Annu. Rev. Biomed. Eng. **3**, 335–373 (2001)

[13] E. Sperling, M. Hohlfeld, M. Mertig: *Soft-lithographically fabricated nanofluidic channels for single-DNA measurements*. Phys. Status Solidi A **212**, 1229–1233 (2015)

[14] S.-M. Park, Y.S. Huh, H.G. Craighead, D. Erickson: *A method for nanofluidic device prototyping using elastomeric collapse*. Proc. Natl. Acad. Sci. U.S.A. **106**, 15549–15554 (2009)

[15] R. Sczech, S. Howitz, M. Mertig: *Diffusion and electrophoretic transport of DNA polymers in microfluidic channels made of PDMS*. Defect Diffus. Forum **312–315**, 1091–1096 (2011)

[16] H. Schmid, B. Michel: *Siloxane polymers for high-resolution, high-accuracy soft lithography*. Macromolecules **33**, 3042–3049 (2000)

[17] *D 263 M cover glass – physical and chemical properties*. Tech. rep., Schott AG

[18] *Ormostamp – product information*. Tech. rep., Micro resist technology

[19] I. Fernandez-Cuesta, A. Laura Palmarelli, X. Liang, J. Zhang, S. Dhuey, D. Olynick, S. Cabrini: *Fabrication of fluidic devices with 30nm nanochannels by direct imprinting*. J. Vac. Sci. Technol. B **29**, 06F801 (2011)

[20] I.J. Malik, S. Pirooz, L.W. Shive, A.J. Davenport, C.M. Vitus: *Surface roughness of silicon wafers on different lateral length scales*. J. Electrochem. Soc. **140**, L75–L77 (1993)

[21] K. Günther, M. Mertig, R. Seidel: *Mechanical and structural properties of YOYO-1 complexed DNA*. Nucleic Acids Res. **38**, 6526–6532 (2010)

[22] C.A. Schneider, W.S. Rasband, K.W. Eliceiri: *NIH Image to ImageJ: 25 years of image analysis.* Nat. Methods **9**, 671–675 (2012)

[23] L.J. Guo, X. Cheng, C.-F. Chou: *Fabrication of size-controllable nanofluidic channels by nanoimprinting and its application for DNA stretching*. Nano Lett. **4**, 69–73 (2004)

[24] M.T.J. van Loenhout, M.V. de Grunt, C. Dekker: *Dynamics of DNA supercoils.* Science **338**, 94–97 (2012)

[25] F. Gittes, C.F. Schmidt: *Signals and noise in micromechanical measurements.* Methods Cell Biol. **55**, 129–156 (1998)

[26] P. Daldrop, H. Brutzer, A. Huhle, D.J. Kauert, R. Seidel: *Extending the range for force calibration in magnetic tweezers.* Biophys. J. **108**, 2550–2561 (2015)

[27] A. Huhle, D. Klaue, H. Brutzer, P. Daldrop, S. Joo, O. Otto, U.F. Keyser, R. Seidel: *Camera-based three-dimensional real-time particle tracking at kHz rates and Ångström accuracy*. Nat. Commun. **6**, 5885 (2015)

[28] A. Crut, D.A. Koster, R. Seidel, C.H. Wiggins, N.H. Dekker: *Fast dynamics of supercoiled DNA revealed by single-molecule experiments.* Proc. Natl. Acad. Sci. U.S.A. **104**, 11957–11962 (2007)

[29] F.W. Schwarz: *The role of 1D diffusion for directional long-range communication on DNA*. Ph.D. thesis, TU Dresden (2012)

[30] H. Brutzer, F.W. Schwarz, R. Seidel: *Scanning evanescent fields using a pointlike light source and a nanomechanical DNA gear.* Nano Lett. **12**, 473–478 (2012)

[31] G. Sasnauskas, G. Kostiuk, G. Tamulaitis, V. Siksnys: *Target site cleavage by the monomeric restriction enzyme BcnI requires translocation to a random DNA sequence and a switch in enzyme orientation.* Nucleic Acids Res. **39**, 8844–8856 (2011)

[32] G. Kostiuk, J. Dikic, F.W. Schwarz, V. Siksnys, R. Seidel: *1D diffusion of the monomeric restriction enzyme BcnI along DNA.* In preparation